Microcavity-integrated graphene photodetector

Furchi, M ; Urich, A ; Pospischil, A ; Lilley, G ; Unterrainer, K ; Detz, H ; Klang, P ; Andrews, A M ; Schrenk, W ; Strasser, G ; Mueller, T

Abstract: There is an increasing interest in using graphene (1, 2) for optoelectronic applications. (3-19) However, because graphene is an inherently weak optical absorber (only 2.3% absorption), novel concepts need to be developed to increase the absorption and take full advantage of its unique optical properties. We demonstrate that by monolithically integrating graphene with a Fabry-Pérot microcavity, the optical absorption is 26-fold enhanced, reaching values >60%. We present a graphene-based microcavity photodetector with responsivity of 21 mA/W. Our approach can be applied to a variety of other graphene devices, such as electro-absorption modulators, variable optical attenuators, or light emitters, and provides a new route to graphene photonics with the potential for applications in communications, security, sensing and spectroscopy.

DOI: https://doi.org/10.1021/nl204512x

NANO LETTERS

Letter

pubs.acs.org/NanoLett

Microcavity-Integrated Graphene Photodetector

Marco Furchi,[†] Alexander Urich,[†] Andreas Pospischil,[†] Govinda Lilley,[†] Karl Unterrainer,[†] Hermann Detz,[‡] Pavel Klang,[‡] Aaron Maxwell Andrews,[‡] Werner Schrenk,[‡] Gottfried Strasser,[‡] and Thomas Mueller*[,†]

[†]Institute of Photonics, Vienna University of Technology, Gußhausstraße 27-29, 1040 Vienna, Austria

[‡]Center for Micro- and Nanostructures, Vienna University of Technology, Floragasse 7, 1040 Vienna, Austria

Supporting Information

ABSTRACT: There is an increasing interest in using graphene[1,2] for optoelectronic applications.[3−19] However, because graphene is an inherently weak optical absorber (only ≈2.3% absorption), novel concepts need to be developed to increase the absorption and take full advantage of its unique optical properties. We demonstrate that by monolithically integrating graphene with a Fabry-Pérot microcavity, the optical absorption is 26-fold enhanced, reaching values >60%. We present a graphene-based microcavity photodetector with responsivity of 21 mA/W. Our approach can be applied to a variety of other graphene devices, such as electro-absorption modulators, variable optical attenuators, or light emitters, and provides a new route to graphene photonics with the potential for applications in communications, security, sensing and spectroscopy.

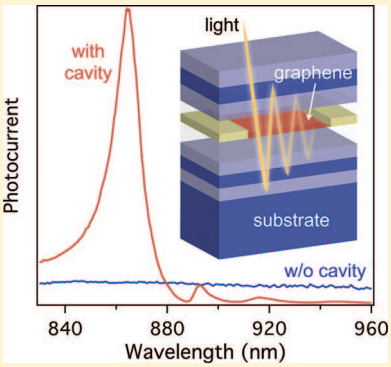

KEYWORDS: *Graphene, photodetector, microcavity, photoresponsivity*

In principle, the light-matter interaction in graphene is strong. The optical absorption coefficient of single-layer graphene[20] is $-\ln(1-\pi\alpha)/d \approx 7 \times 10^5$ cm^{-1}, independent of wavelength (d = 0.335 nm is the thickness of graphene and α is the fine structure constant). At the technologically important wavelengths of 850, 1300, and 1550 nm, this value is between 1 and 3 orders of magnitude higher than that of conventionally used semiconductor materials such as $In_{0.53}Ga_{0.47}As$, GaAs, or Ge.[21] Nevertheless, due to the short interaction length, a layer of graphene absorbs only $\pi\alpha$ = 2.3% of the incident light.[20] Whereas the weak optical absorption is beneficial to devices such as LCD screens,[4,5] solar cells,[6−8] or organic light-emitting diodes,[9] it is detrimental to active optoelectronic devices,[10−18] where a strong light-matter interaction is desired. Several approaches have been pursued to increase the interaction length of light with graphene and enhance the optical absorption. It has been shown that by combining graphene with plasmonic nanostructures[12] or nanoparticles,[13] the near-field enhancement due to localized surface plasmons can significantly increase the responsivity of photodetectors (∼11 and ∼6 mA/W, respectively). The integration of graphene with an optical waveguide allowed the increase of the interaction length through coupling between the evanescent waveguide mode and graphene, resulting in −3 dB (50%) absorption in a ∼30 μm long device.[14] Other approaches to increase absorption are patterning of graphene into an array of nanodisks[15] or layering of several graphene sheets to realize a superlattice.[16] Graphene may also be combined with other photosensitive materials, such as quantum dots,[19] to form a hybrid system for photodetection with extremely high sensitivity (up to 10^8 A/W).

The graphene microcavity photodetectors demonstrated in this letter, benefit from the large increase of the optical field inside a resonant cavity, giving rise to increased absorption. The field enhancement occurs only at the design wavelength, whereas off-resonance wavelengths are rejected by the cavity, making these devices promising for wavelength division multiplexing (WDM) systems.[22] Cavity enhanced devices have a long history in III−V optoelectronics.[23−25] However, monolithic integration of carbon nanomaterials with optical cavities is challenging and experimental realizations are rare.[26,27] Only very recently, a graphene sheet has been incorporated into an optical cavity to study light-matter interactions in a graphene transistor.[27] A graphene device with two coupled optical cavities has been studied theoretically.[28]

Our graphene microcavity photodetector (GMPD) is shown schematically in Figure 1a. As nominal operating wavelength we have chosen λ_c = 850 nm, a wavelength that is often used in low-cost multimode fiber data links.[29] However, due to the broad absorption range of graphene,[20,30] this concept can be extended to any wavelength from the mid-infrared to the ultraviolet, provided that a low-loss optical cavity can be realized at the respective wavelength.[31,32] In our device, two

Received: December 21, 2011
Revised: April 16, 2012
Published: May 7, 2012

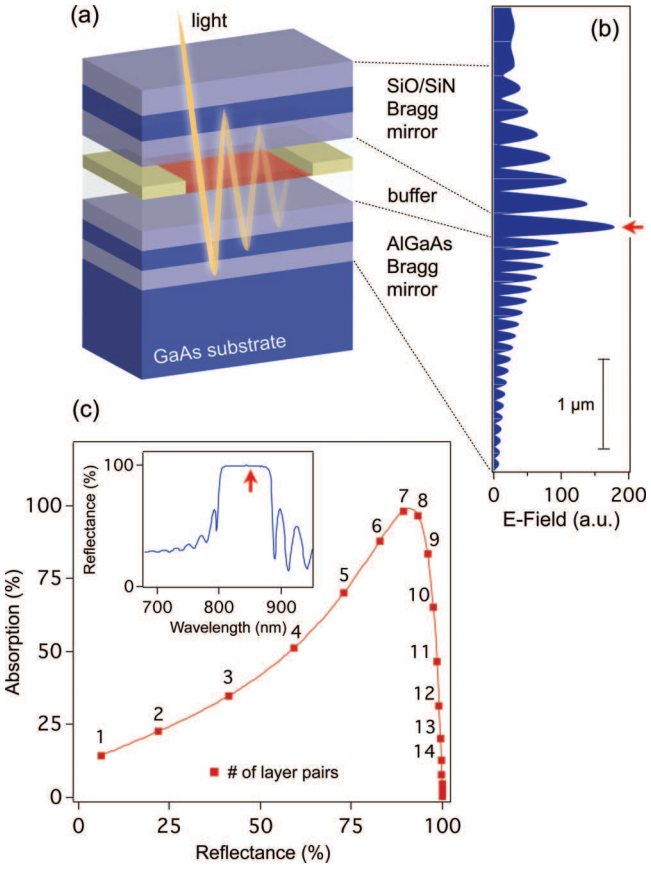

Figure 1. (a) Schematic drawing of a graphene microcavity photodetector. Distributed Bragg mirrors form a high-finesse optical cavity. The incident light is trapped in the cavity and passes multiple times through the graphene. The graphene sheet is shown in red, and the metal contacts are in yellow. (b) Electric field amplitude inside the cavity. (c) Calculated dependence of optical absorption in a single-layer graphene sheet on the reflectivity of the top mirror. The numbers next to the symbols indicate the number of SiO_2/Si_3N_4 layer pairs that are necessary to achieve the respective reflectivity. Inset: Measured reflectivity of the $AlAs/Al_{0.10}Ga_{0.90}As$ bottom mirror.

distributed Bragg mirrors, consisting of quarter-wavelength thick layers of alternating materials with varying refractive indices, form a high-finesse planar cavity. Bragg mirrors are ideal choices for microcavity optoelectronic devices because unlike with metal mirrors the reflectivity can be very well controlled and can reach values near unity. The Bragg mirrors are made of large band gap materials that are nonabsorbing at the detection wavelength λ_c. The absorbing graphene layer is sandwiched between these mirrors. A buffer layer ensures that the maximum of the field amplitude occurs right at the position where the graphene sheet is placed. The bottom mirror is formed from multiple periods (25 pairs) of weakly doped, alternating AlAs and $Al_{0.10}Ga_{0.90}As$ layers (GaAs would be absorbing at 850 nm) with thicknesses of 70 and 61 nm, respectively. It is grown by molecular beam epitaxy (MBE) on an n-doped GaAs substrate. The refractive index contrast of AlAs and $Al_{0.10}Ga_{0.90}As$ gives a mirror with reflectivity $R_{bottom} >$ 99% in a broad spectral range around 850 nm (see inset of Figure 1c). We then deposit a 111 nm thick Si_3N_4 buffer layer by plasma-enhanced chemical vapor deposition (PECVD) using SiH_4 and NH_3 precursor gases at a substrate temperature of 300 °C. Graphene flakes are deposited by mechanical exfoliation. Single- and bilayer flakes are visually located with a microscope and subsequently confirmed to be single- or bilayers with Raman spectroscopy (see Supporting Information). Source and drain Ti/Au (10/20 nm) electrodes are then deposited by laser lithography, electron-beam evaporation of the metals, and lift-off. In a second lithography step, 70 nm thick Au contact pads are patterned. Overnight thermal annealing at 150 °C under vacuum is performed to remove unintentional doping, including water molecules. The annealing is performed in the PECVD chamber, so that the subsequent top Bragg mirror can be deposited without bringing the sample back to atmosphere. The top mirror is made of seven pairs of SiO_2 and Si_3N_4 layers with thicknesses of 147 and 113 nm, respectively. Its nominal reflectivity is 89%. SiH_4 and N_2O are used as precursor gases for the SiO_2 deposition. During all PECVD deposition processes, dummy Si wafers are placed along with the sample into the chamber. This allows precise determination of the film thicknesses by optical measurements (thin film thickness measurements; ellipsometry). Finally, using reactive ion etching (RIE), contact windows are etched in the SiO_2/Si_3N_4 top mirror at the position of the contact pads. The detailed device structure is provided as Supporting Information.

The weak doping of the substrate and the bottom Bragg mirror allows electrostatic gating of the graphene channel and measurements of the electrical characteristics. The devices exhibit the typical V-shaped conductance versus gate bias with weak unintended doping (<10 V Dirac point shift) and negligible hysteresis (<2.5 V). However, we observe a strong mobility reduction to typically a few hundred $cm^2/(V\ s)$, as compared to the ~5000 $cm^2/(V\ s)$ that are obtained in "conventional" graphene devices.[10,11] Similar impact of the dielectric environment on the mobility was previously reported for high-frequency graphene transistors.[33]

The device design was optimized using the transfer matrix method. In our simulation, graphene is described by a complex refractive index $n(\lambda) = 3.0 + i(C_1/3)\lambda$, where $C_1 = 5.446\ \mu m^{-1}$ and λ is the wavelength.[34] The other materials are modeled as loss-less dielectric materials with refractive indices reported in the Supporting Information. Figure 1b shows the electric field distribution in the device for normal incidence light at the design wavelength of $\lambda_c = 850$ nm. The standing wave pattern arises from interference of the counter-propagating incident and reflected waves. The arrow indicates the spatial position of the graphene. It is obvious that the origin of the absorption enhancement is the ~6.5-fold increased electric field amplitude inside the cavity, which causes more energy to be absorbed. An equivalent interpretation is that the photons bounce between the bottom and top mirrors and thus pass multiple times through the graphene sheet as illustrated in Figure 1a. We calculate the wavelength-dependent absorption $A(\lambda)$ according to $A(\lambda) = 1 - R(\lambda) - T(\lambda)$, where $R(\lambda)$ is the (intensity) reflection and $T(\lambda)$ denotes the transmission. The model allows us to optimize the reflectivity R_{top} of the top mirror. As shown in Figure 1c, the absorption increases with increasing reflectivity, reaches a maximum of 98% for seven SiO_2/Si_3N_4 layer pairs (corresponding reflectivity $R_{top} = 89\%$) and drops to zero as R_{top} approaches 100%. This behavior can also be understood intuitively. For small R_{top}, the cavity is too lossy and the field enhancement is small. For $R_{top} = 100\%$, on the other hand, all the light is reflected on the surface and cannot enter into the cavity. For bilayer graphene we find an optimum of six instead of seven SiO_2/Si_3N_4 layer pairs.

The performance of GMPDs depends critically on the optical quality of the mirror and buffer layer materials, which must be

dx.doi.org/10.1021/nl204512x | Nano Lett. 2012, 12, 2773−2777

nonabsorbing at the detection wavelength λ_c. We have therefore measured the wavelength dependent optical reflection of a millimeter-sized spot on the sample. The corresponding spectrum (shown in Figure 2) is a typical reflectivity spectrum

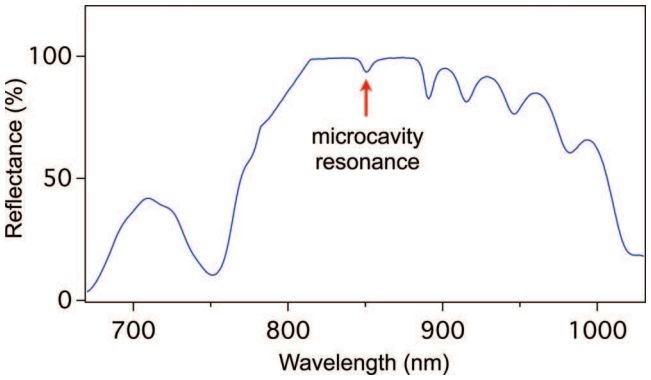

Figure 2. Reflectivity of the sample. The dip at 850 nm wavelength originates from absorption of the Fabry–Pérot microcavity mode.

of a Bragg mirror stack, but exhibits an extra dip at λ = 850 nm in the stop band. The dip originates from absorption of the Fabry–Pérot cavity mode. Its depth is less than 6% and supposedly stems mainly from absorption in the (multilayer) graphene flakes that are randomly distributed over the sample (a few percent surface coverage). The weak absorption is an evidence of the high optoelectronic material quality.

Let us now turn to the photocurrent measurements. Figure 3b shows a microscope image of a single-layer GMPD together with the measurement circuit. The graphene channels of our devices are typically 5 μm long and several micrometers wide. A bias voltage V_{Bias} = 2 V is applied to one of the leads. The other lead is connected to a transimpedance low-noise preamp whose output signal is fed into a lock-in amplifier. The gate electrode (substrate) remains unbiased. The output of a tunable continuous-wave Ti/sapphire laser is set to 850 nm wavelength and is focused with an objective lens to an ~2 μm diameter spot on the sample. The optical power was kept low enough (P = 50 μW) to avoid heating of the sample and reduce the influence of thermo-electric effects.[35−38] A photocurrent map (shown in Figure 3a) is recorded by scanning the laser beam across the sample. The incident light is modulated at 400 Hz using a mechanical chopper. This technique has previously been used to study the potential profiles in graphene transistors, where photocurrents of opposite sign at the metal/graphene interfaces were observed.[39−42] Because of the different biasing condition, the band bending (see Figure 3a) in our experiment is determined by the externally applied voltage, rather than by the metal/graphene contacts. We therefore observe only a single photocurrent peak approximately in the center of the device, whose polarity is determined by the sign of V_B. Although this biasing condition does not allow zero dark current operation, it reduces the influence of the metal electrodes on the shape of the photocurrent spectrum.

In Figure 3c, we present the spectral response of the device. The dashed lines are results of the transfer matrix calculation; the solid lines are measurement results. The reflectivity spectrum is measured by focusing the Ti/sapphire laser output to a small spot in the center of the graphene sheet and by tuning the laser wavelength between 830 and 900 nm. The result is shown in Figure 3c as solid red line. At the cavity

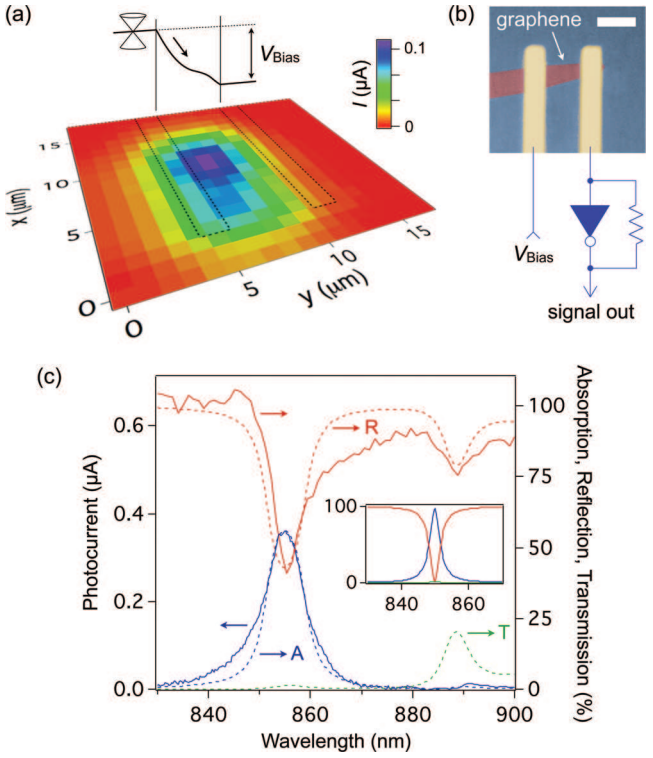

Figure 3. (a) Photocurrent map taken at a bias voltage of V_{Bias} = 2 V between the source and drain electrodes. The gate electrode (substrate) remains unbiased. The dashed lines indicate the source and drain electrodes. The schematic above the photocurrent map illustrates the band diagram under this biasing condition. (b) Microscope image of a graphene photodetector and electrical setup for photocurrent measurements. The scale bar is 5 μm long. (c) Spectral response of the single-layer graphene device. The dashed lines show calculation results: reflection R (red), transmission T (green), and absorption A (blue). The solid lines are measurement results: reflection (red), photocurrent (blue). A strong and spectrally narrow photoresponse is observed at the cavity resonance (855 nm wavelength). Inset: Theoretical result for normal incidence light.

resonance (855 nm), more than 60% of the light is absorbed in the graphene, a 26-fold absorption enhancement as compared to the 2.3% absorption of free-standing graphene.[20] The slight deviation from design wavelength (λ_c = 850 nm) is caused by small nonuniformities (~0.6%) in optical layer thicknesses of the buffer and top mirror layers. We accounted for this deviation in our simulation. At λ = 888 nm another reflection dip is observed, which is, however, not related to absorption in the graphene but stems from larger transmission outside the stop band of the Bragg mirror stack (see green line). The measurement data are well reproduced by the simulation (dashed red line) if we consider spectral broadening due to the finite numerical aperture (NA = 0.28) of the objective lens by numerically averaging over all incidence angles between 0 and ϑ_{max} = Arcsin(NA) ≈ 16°. The solid blue line in Figure 3c shows the spectral photocurrent response of the device. It peaks at λ = 855 nm wavelength and exhibits a spectral width of $\Delta\lambda$ = 9 nm (full width at half-maximum − fwhm). Its shape follows closely the calculated absorption (dashed blue line), demonstrating that the absorbed light is efficiently converted into photocurrent. From the quality factor of the cavity, $Q = \lambda/\Delta\lambda$ = 95, we obtain a photon lifetime of $\tau = Q\lambda/(2\pi c)$ = 43 fs, only. The microcavity does hence not affect the potentially high bandwidth[11,43] of graphene photodetectors. The inset shows

dx.doi.org/10.1021/nl204512x | Nano Lett. 2012, 12, 2773−2777

the calculation results for NA = 0 ($\vartheta_{max} = 0°$), that is, normal incidence light. In this case, the absorption would be as large as 98%.

In Figure 4, we show the results obtained from a bilayer graphene device. The meaning of the curves is the same as in Figure 3c. Again, we observe a strong photoresponse at the cavity resonance (864.5 nm in this case). A peak photocurrent of $I = 1.05\ \mu A$ is obtained at $P = 50\ \mu W$ excitation power, which translates into a photoresponsivity of $S = I/P = 21$ mA/W. Also shown in Figure 4 (solid red line) is the response of a "conventional" bilayer graphene photodetector, that is, a device without cavity. It consists of bilayer graphene on a Si wafer with 300 nm thick SiO_2 and Ti/Au electrodes. For a fair comparison, the geometrical dimensions (particularly the channel length) of the device are similar to those of our GMPD devices and also the biasing conditions are the same. The response of the conventional device is approximately independent of wavelength, but more than an order of magnitude weaker than that of the microcavity enhanced device.

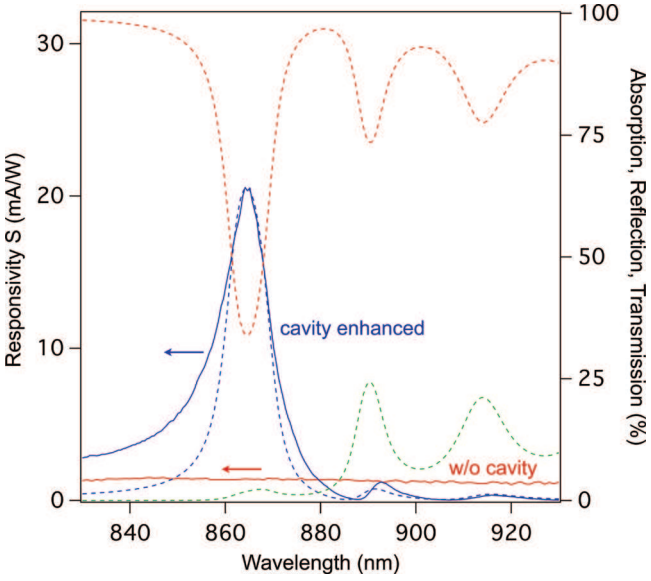

Figure 4. The meaning of the curves is the same as in Figure 3c, but the results are shown for a bilayer graphene device. A maximum responsivity of 21 mA/W is achieved. In addition, the spectral photoresponse of a conventional (without cavity) bilayer graphene detector is shown as solid red line. The response of the conventional device is approximately independent of wavelength, but more than an order of magnitude weaker than that of the microcavity device.

In conclusion, we have demonstrated that the responsivity of a graphene photodetector can be increased by integrating the graphene sheet in a high-finesse planar optical cavity. A responsivity of $S = 21$ mA/W is achieved. The devices show a photoresponse only at the design wavelength, making them promising for wavelength division multiplexing. The concept of enhancing the light-matter interaction in graphene by use of an optical microcavity is not limited to photodetectors alone. It can be applied to a variety of other devices such as electroabsorption modulators, variable optical attenuators, and possibly future light emitters. Our demonstration also shows that graphene can be monolithically integrated with other, more established materials and technologies to form novel, highly complex devices.

■ ASSOCIATED CONTENT

Supporting Information

Detailed device structure and Raman spectrum. This material is available free of charge via the Internet at http://pubs.acs.org.

■ AUTHOR INFORMATION

Corresponding Author

*E-mail: thomas.mueller@tuwien.ac.at.

Notes

The authors declare no competing financial interest.

■ ACKNOWLEDGMENTS

This work was supported by the Austrian Science Fund FWF (START Y-539) and the Austrian Research Promotion Agency FFG (NIL-Graphene).

■ REFERENCES

(1) Novoselov, K. S.; Geim, A. K.; Morozov, S. V.; Jiang, D.; Zhang, Y.; Dubonos, S. V.; Grigorieva, I. V.; Firsov, A. A. *Science* **2004**, *306*, 666−669.

(2) Novoselov, K. S.; Geim, A. K.; Morozov, S. V.; Jiang, D.; Katsnelson, M. I.; Grigorieva, I. V.; Dubonos, S. V.; Firsov, A. A. *Nature* **2005**, *438*, 197−200.

(3) Bonaccorso, F.; Sun, Z.; Hasan, T.; Ferrari, A. C. *Nat. Photonics* **2010**, *4*, 611−622.

(4) Blake, P.; Brimicombe, P. D.; Nair, R. R.; Booth, T. J.; Jiang, D.; Schedin, F.; Ponomarenko, L. A.; Morozov, S. V.; Gleeson, H. F.; Hill, E. W.; Geim, A. K.; Novoselov, K. S. *Nano Lett.* **2008**, *8*, 1704−1708.

(5) Bae, S.; Kim, H.; Lee, Y.; Xu, X.; Park, J.-S.; Zheng, Y.; Balakrishnan, J.; Lei, T.; Kim, H. R.; Song, Y. I.; Kim, Y.-J.; Kim, K. S.; Özyilmaz, B.; Ahn, J.-H.; Hong, B. H.; Iijima, S. *Nat. Nanotechnol.* **2010**, *5*, 574−578.

(6) Wang, X.; Zhi, L.; Tsao, N.; Tomović, Ž.; Li, J.; Müllen, K. *Angew. Chem.* **2008**, *47*, 2990−2992.

(7) Wu, J.; Becerril, H. A.; Bao, Z.; Liu, Z.; Chen, Y.; Peumans, P. *Appl. Phys. Lett.* **2008**, *92*, 263302.

(8) De Arco, L. G.; Zhang, Y.; Schlenker, C. W.; Ryu, K.; Thompson, M. E.; Zhou, C. *ACS Nano* **2010**, *4*, 2865−2873.

(9) Wu, J.; Agrawal, M.; Becerril, H. A.; Bao, Z.; Liu, Z.; Chen, Y.; Peumans, P. *ACS Nano* **2010**, *4*, 43−48.

(10) Mueller, T.; Xia, F.; Avouris, Ph. *Nat. Photonics* **2010**, *4*, 297−301.

(11) Xia, F.; Mueller, T.; Lin, Y.; Valdes-Garcia, A.; Avouris, Ph. *Nat. Nanotechnol.* **2009**, *4*, 839−843.

(12) Echtermeyer, T. J.; Britnell, L.; Jasnos, P. K.; Lombardo, A.; Gorbachev, R. V.; Grigorenko, A. N.; Geim, A. K.; Ferrari, A. C.; Novoselov, K. S. *Nat. Commun.* **2011**, *2*, 458.

(13) Liu, Y.; Cheng, R.; Liao, L.; Zhou, H.; Bai, J.; Liu, G.; Liu, L.; Huang, Y.; Duan, X. *Nat. Commun.* **2011**, *2*, 579−585.

(14) Liu, M.; Yin, X.; Ulin-Avila, E.; Geng, B.; Zentgraf, T.; Ju, L.; Wang, F.; Zhang, X. *Nature* **2011**, *474*, 64−67.

(15) Thongrattanasiri, S.; Koppens, F. H. L.; García de Abajo, F. J. *Phys. Rev. Lett.* **2012**, *108*, 047401.

(16) Yan, H.; Li, X.; Chandra, B.; Tulevski, G.; Wu, Y.; Freitag, M.; Zhu, W.; Avouris, Ph.; Xia, F. *Nat. Nanotechnol.* **2012**; DOI: 10.1038/nnano.2012.59.

(17) Zhang, H.; Tang, D. Y.; Zhao, L. M.; Bao, Q. L.; Loh, K. P. *Opt. Express* **2009**, *17*, 17630−17635.

(18) Sun, Z.; Hasan, T.; Torrisi, F.; Popa, D.; Privitera, G.; Wang, F.; Bonaccorso, F.; Basko, D. M.; Ferrari, A. C. *ACS Nano* **2010**, *4*, 803−810.

(19) Konstantatos, G.; Badioli, M.; Gaudreau, L.; Osmond, J.; Bernechea, M.; Garcia de Arquer, P.; Gatti, F.; Koppens, F. H. L. Arxiv:1112.4730v1.

(20) Nair, R. R.; Blake, P.; Grigorenko, A. N.; Novoselov, K. S.; Booth, T. J.; Stauber, T.; Peres, N. M. R.; Geim, A. K. *Science* **2008**, *320*, 1308.
(21) *Handbook of Optical Constants of Solids*; Palik, E. D., Ed.; Academic Press: New York, 1985.
(22) Ishio, H.; Minowa, J.; Nosu, K. *J. Lightwave Technol.* **1984**, *2*, 448−463.
(23) Ünlü, M. S.; Strite, S. *J. Appl. Phys.* **1995**, *78*, 607−638.
(24) Schubert, E. F.; Wang, Y.-H.; Cho, A. Y.; Tu, L.-W.; Zydzik, G. J. *Appl. Phys. Lett.* **1992**, *60*, 921−923.
(25) Maier, T.; Strasser, G.; Gornik, E. *IEEE Photonics Technol. Lett* **2000**, *12*, 119−121.
(26) Xia, F.; Steiner, M.; Lin, Y.; Avouris, Ph. *Nat. Nanotechnol.* **2008**, *3*, 609−613.
(27) Engel, M.; Steiner, M.; Lombardo, A.; Ferrari, A. C.; Loehneysen, H.; Avouris, Ph.; Krupke, R. *Nat. Nanotechnol.* **2012**; DOI: 10.1038/nnano.2012.60.
(28) Ferreira, A.; Peres, N. M. R.; Ribeiro, R. M.; Stauber, T. *Phys. Rev. B* **2012**, *85*, 115438.
(29) Pepeljugoski, P.; Kuchta, D.; Kwark, Y.; Pleunis, P.; Kuyt, G. *IEEE Photonics Technol. Lett.* **2002**, *14*, 717−719.
(30) Mak, K. F.; Sfeir, M. Y.; Wu, Y.; Lui, C. H.; Misewich, J. A.; Heinz, T. F. *Phys. Rev. Lett.* **2008**, *101*, 196405.
(31) Heiss, W.; Schwarzl, T.; Roither, J.; Springholz, G.; Aigle, M.; Pascher, H.; Biermann, K.; Reimann, K. *Prog. Quantum Electron.* **2001**, *25*, 193−228.
(32) Dorsaz, J.; Carlin, J.-F.; Gradecak, S.; Ilegems, M. *J. Appl. Phys.* **2005**, *97*, 084505.
(33) Lin, Y.; Jenkins, K. A.; Valdes-Garcia, A.; Small, J. P.; Farmer, D. B.; Avouris, Ph. *Nano Lett.* **2009**, *9*, 422−426.
(34) Bruna, M.; Borini, S. *Appl. Phys. Lett.* **2009**, *94*, 031901.
(35) Xu, X.; Gabor, N. M.; Alden, J. S.; van der Zande, A. M.; McEuen, P. L. *Nano Lett.* **2010**, *10*, 562−566.
(36) Lemme, M. C.; Koppens, F. H. L.; Falk, A. L.; Rudner, M. S.; Park, H.; Levitov, L. S.; Marcus, C. M. *Nano Lett.* **2010**, *11*, 4134−4137.
(37) Gabor, N. M.; Song, J. C. W.; Ma, Q.; Nair, N. L.; Taychatanapat, T.; Watanabe, K.; Taniguchi, T.; Levitov, L. S.; Jarillo-Herrero, P. *Science* **2011**, *334*, 648−652.
(38) Prechtel, L.; Song, L.; Schuh, D.; Ajayan, P.; Wegscheider, W.; Holleitner, A. W. *Nat. Commun.* **2012**, *3*, 646−652.
(39) Lee, E. J. H.; Balasubramanian, K.; Weitz, R. T.; Burghard, M.; Kern, K. *Nat. Nanotechnol.* **2008**, *3*, 486−490.
(40) Xia, F.; Mueller, T.; Golizadeh-Mojarad, R.; Freitag, M.; Lin, Y.; Tsang, J.; Perebeinos, V.; Avouris, Ph. *Nano Lett.* **2009**, *9*, 1039−1044.
(41) Mueller, T.; Xia, F.; Freitag, M.; Tsang, J.; Avouris, Ph. *Phys. Rev. B* **2009**, *79*, 245430.
(42) Park, J.; Ahn, Y. H.; Ruiz-Vargasv, C. *Nano Lett.* **2009**, *9*, 1742−1746.
(43) Urich, A.; Unterrainer, K.; Mueller, T. *Nano Lett.* **2011**, *11*, 2804−2808.